Construction and Building Materials 261 (2020) 120492

Contents lists available at ScienceDirect

Construction and Building Materials

journal homepage: www.elsevier.com/locate/conbuildmat

A study on ASR mitigation by optimized particle size distribution

İlhami Demir [a], Burak Sivrikaya [b], Ozer Sevim [a,*], Mehmet Baran [c]

[a] Department of Civil Engineering, Kırıkkale University, Kırıkkale 71451, Turkey
[b] Kaman Vocational School, Building Inspection, Kırşehir Ahi Evran University, Kırşehir 40360, Turkey
[c] Department of Civil Engineering, Yıldırım Beyazıt University, Ankara 06050, Turkey

HIGHLIGHTS

- Effect of ASR on cement-based systems having optimized PSD have been investigated.
- Specimens have been exposed to ASR effect according to ASTM C227 and ASTM C1260.
- The characterization of specimens was investigated using the SEM, FTIR and TGA.
- FA and slag additive with optimized PSD were found to be effective in reducing ASR.

ARTICLE INFO

Article history:
Received 12 May 2020
Received in revised form 30 July 2020
Accepted 4 August 2020
Available online 28 August 2020

Keywords:
Alkali-silica reaction
Cementitious composites
Fly ash
Blast furnace slag
Particle size distribution FTIR
TGA

ABSTRACT

In this study, the effect of alkali-silica reaction on binary cementitious composite systems incorporating fly ash or slag having optimized particle size distribution has been investigated. Specimens have been exposed to ASR effect according to ASTM C227 and ASTM C1260 methods. Test results, which were conducted after ASR exposure, have been discussed in terms of use of additive having optimized particle size distribution. The characterization of specimens was investigated using scanning electron microscopy (SEM) coupled with energy dispersive X-ray spectroscopic analyzer (EDS), Fourier-transform infrared spectroscopy (FTIR) and thermogravimetric analysis instrument (TGA). As a result of the experimental program, it was seen that the ASR effect is reduced with fly ash and slag replacement. Even, fly ash addition has been more effective than slag addition in reducing the ASR effect for the same additive ratio. In addition, addition of fly ash and slag with optimized particle-size distribution were found to be more effective in reducing the ASR effect as compared to addition of fly ash and slag without optimized particle-size distribution.

1. Introduction

Concrete is one of the most important construction materials that structurally support buildings and is the most used one. After its construction, a reinforced concrete building should be protected against external exposures. Environmental factors as climate change, freeze–thaw effects, reinforcement corrosion and chemical factors as alkali-silica reaction (ASR) and sulfate effect can be counted as external exposures.

ASR starts by forming alkali-silica gel with high water absorption capacity when alkali oxides in cement ($Na_2O + 0.658 \times K_2O$) and reactive silica in aggregate (SiO_2) go into a chemical reaction [1]. Formed gels expand when they absorb large amount of water available in a moist environment and it continues by increasing concrete internal stresses due to volume expansion stemming from gel expansion. Concrete starts to deteriorate and loses strength as a result of increased internal stresses.

There exist too many studies on the relationship between material design and ASR for high strength concrete. In these studies, it is generally stated that the use of mineral additives can provide protection against damage caused by ASR due to low porosity and water to cement ratio effect [2,3].

There are several approaches to prevent ASR. First, elimination of one or more of factors such as moisture, reactive silica and alkali can be considered as a precaution. In addition, damage given by the reaction can also be reduced using mineral and chemical additives [4–10]. There are several materials effective in preventing ASR. These materials can be lithium-based salts, silica fume as mineral additives, blast furnace slag (BFS), fly ash (FA) and rice husk ash.

Pozzolans reduce the pH content of the cement mortar by keeping hold of the lime. Low pH content reduces the solubility of silica and prevents the formation of alkali-silica gel. Besides, pozzolans

* Corresponding author.
E-mail address: ozersevim@kku.edu.tr (O. Sevim).

https://doi.org/10.1016/j.conbuildmat.2020.120492
0950-0618/

also increase the impermeability of concrete [11]. In the structure of gel, CaO always exists. Lack of CaO does not indicate that gel will not form. It can be said that pozzolans prevent the formation of gel by binding CaO [12].

Hasparyk et al. (2003) [13] and Mehta (1985) [14] have reported that less alkali-silica reactions have occurred in concrete specimens produced with silica fume (SF) by weight of cement due to slightly lower amount of alkali formed in concrete. In some studies, it was observed that the use of FA and BFS has reduced the ASR effect [2,15,16].

C-S-H phases of FA are low with respect to calcium due to pozzolanic reactions of FA, in other words, it has a low FA/SiO_2 ratio and thus has a high alkali binding capacity. FA which was found to be most effective in reducing the alkalinity of the pore solution expressed from cementitious composite samples was also found to be the best for controlling ASR expansion [17].

The formation of alkali in the resulting reaction products in FA containing binders begins simultaneously with the pozzolanic reaction, i.e., resulting in a consecutive decrease in the dissolvable alkali content at the end of approximately 28 days. FA with low CaO content reduces the alkalinity of the pore solution only just beyond the dilution level [18]. As compared to the first 28 days, it is thought that the differences in linear extension in between the pozzolan substituted mortar bars and the additive-free cementitious mortar bars, relatively larger rates of differences, are due to the decrease in the alkaline content of the cement at the end of 28-day period.

As well as FA and BFS addition processes makes economy in concrete usage, it extends the setting time of concrete, lowers hydration heat as a result of slowing of concrete setting and prolonging of its setting time and it is known to increase concrete strength for over 90 days [19–27].

Concrete is a construction material where its strength increases as the void ratio decreases. Final products formed as a result of hydration in concrete are not enough in filling these voids and have negative effects in terms of its strength. There are studies in which compactness optimization of the filler materials' particle size distribution is increased with the aim of increasing compactness of concrete production [28–30].

Having carried out a thorough literature review, it was found that there exists a lack of research on mitigation of ASR using optimized powdery material gradations such as fly ash and blast furnace slag. Previous studies have commonly focused on the effect of the utilization of mineral additives such as fly ash and slag. To date, there is a lack of research on the optimal designs aimed to obtain high compactness using powder material gradation with pozzolans, such as fly ash and slag. The selection of PSD requires a focus on the ability to fill in the voids among particles. On the basis of the aforementioned information, designs were made to obtain the optimal fly ash or slag PSD to obtain the highest compactness. It is possible to achieve a mixture of materials at suitable percentages, which have low void ratio and high compactness. This research is important from the point of view of showing how much ASR effect can be reduced using 0–20% BFS and FA with optimized particle size distribution. In this study, the effect of alkali-silica reaction on binary cementitious composite systems incorporating fly ash or slag having optimized particle size distribution have been investigated. Specimens have been exposed to ASR effect according to ASTM C227 and ASTM C1260 methods. Test results, which were conducted after ASR exposure, have been discussed in terms of use of additive having optimized particle size distribution.

2. Experimental program

2.1. Materials

CEM I 42.5 R type ordinary portland cement (OPC), aggregate, BFS and FA were used in this study. Physical properties and chemical compositions of the cement, aggregate, FA and BFS used are shown in Table 1.

In the experimental study, CEM I 42.5 R type cement with an alkali ratio greater than 0.6% was used. İzmir Gediz River aggregate was used as aggregate. FA classified as F class according to ASTM C618 [10] was used in this study. BFS obtained from Bolu cement was used. Aggregate used in the experimental study was prepared by sieving according to the particle size analyses defined in ASTM C227 [31] and ASTM C1260 [32].

Table 1
Physical and chemical properties of the cement, aggregate, FA and BFS.

Chemical Composition (%)	Cement	Aggregate	FA	BFS
SiO_2	18.79	73.05	57.11	42.40
Al_2O_3	5.05	7.31	19.27	12.56
Fe_2O_3	2.54	3.34	9.21	1.03
CaO	63.28	5.46	5.31	35.04
MgO	2.23	0.68	2.03	5.11
K_2O	0.83	1.49	2.39	0.75
Na_2O	0.28	0.06	0.64	0.14
SO_3	3.44	–	0.13	0.37
Loss of ignition	3.20	–	3.24	0.21
$Na_2O + 0.658 \times K_2O$	0.82	–	–	–
Specific surface area (cm^2/g)	3220	–	2695	3594
Specific Surface area (Optimized) (cm^2/g)	–	–	2943	3722

Table 2
Mixture rates of optimized particle size analysis for FA and BFS (g).

Additive ratio (%)	Sieve diameter (μm)				
	0–25	25–38	38–45	45–53	53–63
5	15.20	2.77	1.26	1.30	1.47
10	30.40	5.54	2.52	2.60	2.94
15	45.60	8.31	3.77	3.90	4.41
20	60.80	11.09	5.03	5.20	5.88

2.2. Methods

2.2.1. Particle size distribution of fly ash and blast furnace slag

The most suitable sieve size analysis for PSD optimization was determined by using Eq. (1) suggested for PSD optimization in the study conducted by Dinger and Funk [33]. Maximum particle size diameter was determined to be 63 μm for FA and BFS. Sieve diameter to be used was selected as 25, 38, 53 and 63 μm. Required particle size analysis was carried out by using Eq. (1) and given in Table 2.

$$P(D) = \frac{D^q - D^q_{min}}{D^q_{max} - D^q_{min}} \times 100 \quad (1)$$

where P(D) is material passing through the sieve with spacing D, D is the sieve diameter, D_{max} is the maximum particle size diameter of powder materials, and q is particle distribution modulus.

Increasing the value of the distribution modulus results in a rather coarse-grained mixture; on the other hand, decreasing this value results in a rather fine-grained mixture. The optimal PSD of fly ash and blast furnace slag was calculated for different values of the distribution modulus q using Eq. (1) where value of q ranged from 0 to 1 with constant increments of 0.1. High compactness was ensured through the filler effect for the value of distribution modulus is equal to 0.4 offering higher compressive and flexural strengths at 7, 28 and 90 days in our previous papers [28–30]. Sevim and Demir [28,29] has determined the maximum compressive and flexural strengths and durability properties for q = 0.4 particle distribution module in the PSD optimization of FA study. As can be seen in this study, particle distribution module value of 0.4 was used while making PSD optimization.

FA and BFS with optimized PSD (for q = 0.4) was obtained by sieving using vacuum sieve and was mixed at the rates given in Table 2. PSD curves of the FA, BFS, optimized-FA (O-FA) and optimized-BFS (O-BFS) used in this study are given in Fig. 1.

2.2.2. Accelerated mortar-bar test method

The accelerated mortar-bar test method is a short time testing method in which results are obtained in 16 days according to ASTM C1260 [32]. Prismatic mortar bars having dimensions of 25 mm × 25 mm × 285 mm were prepared according to the gradation defined in ASTM C1260, where the ratio of the amount of aggregate to that of the cement and water to cement ratio corresponded to be 2.25 and 0.47, respectively. After pouring, test specimens were left in the mold for 24 h and then taken out from the mold. Specimens taken out molds were placed in a 1 N NaOH solution at 80 °C for 24 h. The solution of 1 N NaOH was obtained by mixing of 40 g NaOH into 900 g water. NaOH was dissolved and diluted with additional distilled or deionized water to obtain 1.0 L of solution. The first measurement on the specimens was conducted after this period and the specimens were again placed in the solution at 80 °C for 14 days. The test was finalized by reading the length change at the end of this 14-day period [32].

2.2.3. Standard mortar-bar test method

The standard mortar-bar test method is an experimental method that determines the effects of ASR by measuring the expansion values at the end of 12-month period stemming from ASR of mineral and chemical additives causing length change according to ASTM C227 [31]. For ASTM C227 test method, at least 3 specimens having dimensions of 25 mm × 25 mm × 285 mm for each mix were prepared, where the mass of aggregate was 2.25 times to that of cement and the water to cement ratio corresponded to be 0.47. After the cast into molds, specimens were left in them for 24 h. Taking out of the specimens from the molds after 24 h, first measurements were conducted, and specimens were kept at 38 °C in the moisture cabinet prepared such that no contact occurred in between specimens and the curing water. The length change values of specimens at the end of 2, 7, 28, 90, 180 and 360-days were measured, and length change values were calculated. Comparison of the test methods followed in the experiments is given Table 3.

2.2.4. Characterization of the specimens

The morphology of the specimens was examined using scanning electron microscopy (SEM) coupled with energy dispersive X-ray spectroscopic analyzer (EDS). For performing the microstructure surface inspection, specimens were applied gold coating with Sputter Coater. The specimens were investigated by scanning electron microscopy. For the microstructure analysis, Quanta 450 FEG

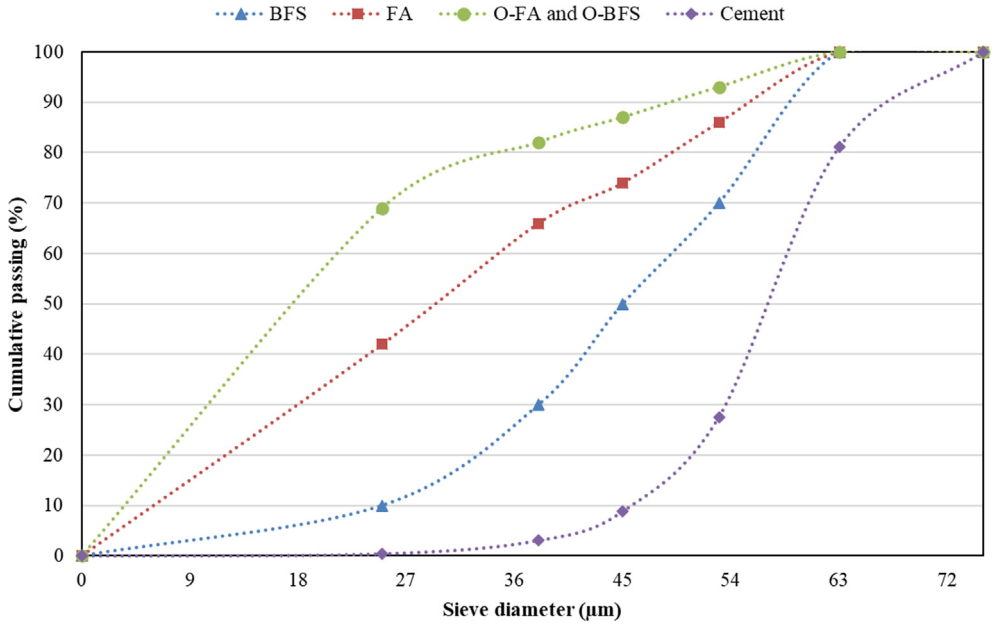

Fig. 1. Particle size distribution (PSD) curves of the cement, fly ash and blast furnace slag.

Table 3
Comparison of test methods defined in ASTM C1260 and ASTM C227.

Method	ASTM C1260	ASTM C227
Specimen design	Mortar Bar 25 × 25 × 285 mm	Mortar Bar 25 × 25 × 285 mm
Water to cement ratio	0.47	Not Specified
Sand-cement ratio	2.25	2.25
Curing conditions	80 °C 1 N NaOH solution	38 °C %100 relative humidity
Duration of testing	14-day	12-month
Examination of the results	Detrimental zone > 0.2% 0.2%>controlled zone > 0.1% 0.1% > Non-detrimental zone	Detrimental zone > 0.1% 0.1% > Non-detrimental zone

scanning electron microscopy (SEM) was used. EDS analyses were carried out at 35× magnification.

The bond vibrations to study the effect of the specimens was carried out with FTIR spectrometer (Fourier-transform infrared spectroscopy) equipment. In the FTIR analysis, investigation of the individual spectra allows for determining a chemical compound in the specimen. When infrared light passes through the specimen, each functional group resonates in its characteristic absorption frequencies of the spectra. Obtained data represents the fingerprint of the bound between the molecules.

The reaction products to study the effect of the specimens were investigated with a thermogravimetric analysis instrument (TGA). The temperature was set to increase at a rate of 20 °C/min from room temperature to 1000 °C. Temperature as a function of a thermogram was recorded to provide qualitative and quantitative information.

3. Research findings

3.1. Accelerated mortar bar test results

Specimens prepared according to the accelerated test method were tested according to ASTM C1260 [32] and length changes were given in Fig. 2. In this test, the highest length change value was observed in specimens without a pozzolan addition called "control". As a result of the measurements, control specimens were identified as detrimental in terms of ASR according to ASTM C1260.

From 5% pozzolan substituted mortar-bar point of view, BFS substituted mortar bars have the highest length change whereas optimized fly ash (O-FA) mortar bars have the lowest rate. PSD optimization summarized the length change effect as can be seen in Fig. 2. When the length change of the 10% substituted mortar bars given in Fig. 2 is examined, it is seen that the length change in parallel with that of the 5% substituted ones. Mortar bars with 10% BFS addition have the highest length change, while the lowest length change has been achieved in mortar bar with 10% O-BFS. Mortar bars with 10% O-FA remained in the non-detrimental zone from the ASR point of view, while other bars with 10% addition remained in the controlled zone for ASR.

According to Fig. 2; the highest length change was observed in mortar bars with BFS whereas lowest length change was observed in O-FA substituted mortar bars. While 15% FA and 15% O-FA substituted mortar bars remained in the non-detrimental zone in terms of ASR, BFS substituted ones remained in the controlled zone for ASR. From 20% pozzolan substituted mortar bars point of view, BFS substituted mortar bars remained in the controlled zone for ASR, while O-BFS remained in the non-detrimental zone in terms of ASR. Mortar bars with 20% FA remained in the non-detrimental zone for ASR. As can be seen in Fig. 2, it was observed that 20% O-FA addition reduces the ASR.

When length changes of FA and O-FA substituted mortar bars are examined, it is seen that O-FA is effective in reducing the ASR with the filling effect besides the chemical effect. The use of FA has been seen to be more effective in reducing the ASR than the use of BFS for the same additive ratio. Optimizing PSD for BFS and FA (O-BFS and O-FA) was found to be more effective in reducing the ASR effect on mortar bars. Among the prepared specimens, the control specimen took the highest ASR damage whereas the most harmless specimen in terms of ASR was found to be 20% O-FA substituted mortar bars.

This result showed that FA and BFS with optimized PSD are effective in preventing ASR by increasing the filling effect. An increase in filling effect reduced the void ratio and permeability in concrete. With the decrease in the void ratio in concrete, the formation of alkali-silica gels and the effect of ASR are reduced.

3.2. Standard mortar bar test results

The length changes of cement mortar bars prepared according to ASTM C 227 [31] were measured at the end of 7, 14, 28, 90, 180 and 360 days and the length changes of the mortar bars were obtained. Since the values for 7 and 28 days are close to 0.00, the values for 90, 180 and 360 days are given comparatively. The length changes of cement mortar bars are given Figs. 3–6.

Fig. 3 demonstrates the length changes of the mortar bar having BFS. As can be seen in Fig. 3, low length change was observed in the

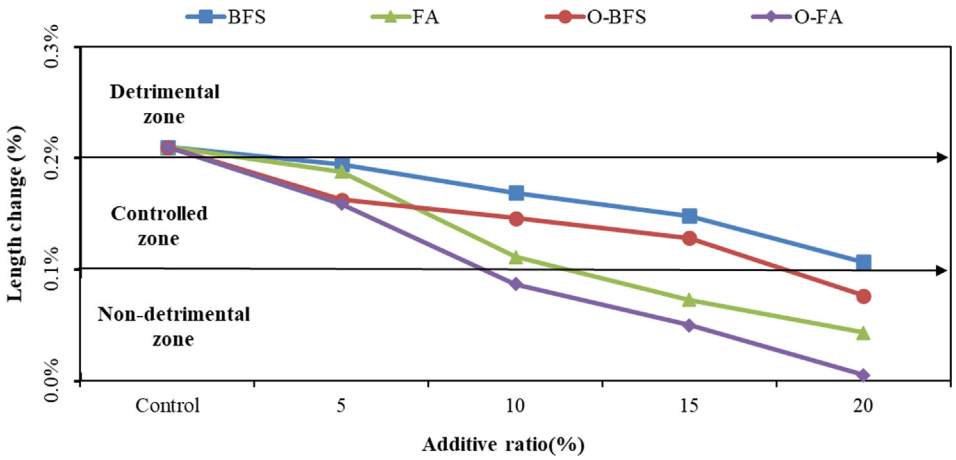

Fig. 2. Length changes of BFS, FA, O-BFS and O-FA added mortar bars in 14 days.

control specimen at early age in which the highest length change occurred at the end of the first month among the mortar bar specimens. The control specimen had shown a length change of 0.1689% in 180 days where this value was 0.1761% at the end of 360 days. According to ASTM C227, specimens with an increase in length change of more than % 0.1 at the end of 360 days are considered as detrimental in terms of ASR and control specimen was accepted to be non-detrimental in terms of ASR according to the ASTM C227 values given in Table 3. The control specimen showed detrimental ASR effect after 180 days.

As can be seen in Fig. 3, a value of 0.134% for length change was seen in BFS5 for 360 days. It was considered to be detrimental in terms of ASR because of its length change greater than 0.1%. Compared to the control specimen, there occurred to be 24.1% reduction in the length change. At the end of 360 days, a value of 0.125% for length change was observed in 10% BFS substituted mortar bars. As compared to the control specimen, length change has decreased by 29.3%. Since length change came out to be greater than 0.1%, it was considered to be detrimental in terms of ASR. In the case of 15% BFS substituted mortar bars, a value of 0.121% for length change was observed at the end of 360 days and it was classified to be detrimental in terms of ASR. It provided a value of 31.2% reduction in length change as compared to the control specimen. The length change came out to be 0.106% at the end of 360 days in 20% BFS substituted mortar bars and showed a very close value to that of limit from an assessment point of view. However, it was classified as detrimental in terms of ASR since the length change was greater than 0.1%. The detrimental effect of ASR on BFS substituted mortar bars was first seen on 5% substituted ones on the 90-day. At the end of 180 days, BFS substituted mortar bars showed detrimental effect in terms of ASR.

Fig. 4 demonstrates the length changes of the mortar bar having O-BFS. As can be seen in Fig. 4, a value of 0.127% for length change was observed in 5% O-BFS substituted mortar bars. A reduction of 28.11% in was observed in length change as compared to the control specimen and it was considered as detrimental in terms of ASR since length change was greater than 0.1%. Substituting 10% O-BFS provided a value of 0.122% for length change ratio at the end of 360 days and a decrease of 30.7% as compared to that of the control specimen. As can be seen in Fig. 4, performing 10% O-BFS addition was not sufficient to make ASR effect non-detrimental and remained in the detrimental zone in terms of ASR. The length change of 0.102% was observed in the case of 15% O-BFS addition, and length change increase of 0.1% limit value occurred in terms of ASR. As compared to the control specimen, there occurred to be a 42.09% decrease in length change. As shown in Fig. 4, a length change of 0.095% was measured in mortar bars with 20% O-BFS addition which were classified as non-detrimental in terms of ASR since the length change stayed below the limit value of 0.1%. When O-BFS substituted mortar bars are examined in general, mortar bars of 5%, 10% and 15% O-BFS addition showed a detrimental effect at the end of 90, 180 and 360 days, respectively. Since the limit value for length change in terms ASR is defined as 0.1% in Table 3, 20% O-BFS substituted mortar bars stayed below this limiting value and classified as non-detrimental. When the 360-day experimental results given in Fig. 3 and Fig. 4 are examined, although 15% and 20% BFS substituted cement mortar bars were in the detrimental zone in terms of ASR, same proportion of O-BFS substituted ones remained in the non-detrimental zone in terms of ASR. These results show that the use of BFS with optimized PSD is more effective in preventing ASR than the use of BFS without optimized PSD. In other words, the filling effect was more useful in preventing ASR.

Fig. 5 demonstrates the length changes of the mortar bar having FA. As given in Fig. 5, 0.124% length change was detected in 5% FA substituted mortar bars as a result of 360-day readings. The addition of 5% FA with non-optimized PSD has achieved a 29.3% reduction in length change as compared to the control specimen after 360-day. However, this value of FA addition fell short of decreasing the length change below 0.1% as specified in ASTM C227 and length change remained above the limiting value as a result of 360-day. Therefore, it was considered as detrimental in terms of ASR.

In 360-day readings on mortar bars with 10% FA, 0.107% length change value was obtained. As a result of the evaluations, it was observed that there was a 47.93% reduction in 360-day length change ratios as compared to the control specimen. In the case of 15% FA substituted mortar bars, 360-day length change was found to be 0.11%. 15% FA addition with non-optimized PSD into cement mortar bars had achieved a 36.9% reduction in 360-day length change. According to ASTM C227, 15% FA with non-optimized PSD substituted cement mortar bars are classified as detrimental in terms of ASR since length change remains above 0.1% as a result of 360-day readings. It has determined that 20% FA substituted mortar bars had a length change of 0.092% at the end of 360 days. It was observed addition of 20% FA into the mortar bars decreased the length change ratio by 47.9% as compared to the control specimen at the end of 360 days and was observed to be non-detrimental in terms of ASR. Harmful effects of ASR were not observed until the 180-day in the case of FA with non-optimized PSD substituted specimens. At the end of 180-day, 5% and 10% FA substituted mortar bars started to show detrimental effects in terms of ASR. At the end of 360 days, 20% FA substituted mortar bars were considered as non-detrimental according to Table 3.

Fig. 6 demonstrates the length changes of the mortar bar having O-FA. As it is given in Fig. 6, length change of 0.113% was determined after 360 days for 5% FA with optimized PSD substituted mortar bars. As compared to the control specimen, a decrease ratio of 35.9% was recorded in length change of mortar bars after 360 days. Since mortar bars with 5% FA with optimized PSD had length change above the limiting value given in ASTM C227, they were classified as detrimental in terms of ASR.

As a result of length change measurements made in mortar bars with 10% FA addition with optimized PSD, 0.098% value was obtained in 360-day period. As compared to the control specimen, mortar bars with 10% FA with optimized PSD showed a decrease of 44.40% in length change after 360-day period readings and was classified as non-detrimental in terms of ASR. There occurred a decrease of nearly 48.8% in length change for 15% FA addition with optimized PSD as compared to the control specimen and was classified as non-detrimental in terms of ASR since length change of 0.900% was obtained at the 360-day reading. The length change was obtained as 0.0822% at the 360-day reading for 20% FA with optimized PSD substituted mortar bars, as given in Fig. 6. A decrease of 53.4% value was obtained in readings after 360 days and they were classified as non-detrimental in terms of ASR. After 180 days, length change came out to be higher than the limiting value of 0.1% for 5% FA with optimized PSD substituted mortar bars so they showed detrimental effect in terms of ASR. At the end of 360 days, 5% FA with optimized PSD substituted mortar bars showed detrimental ASR effect while %10, %15 and %20 FA with optimized PSD substituted mortar bars stayed in the non-detrimental zone in terms of ASR. Mortar bars of 10%, 15% and 20% FA addition with optimized PSD were found to be more effective in reducing the ASR effect as compared to mortar bars with non-optimized PSD. While 10% FA with non-optimized PSD substituted mortar bars passed into the detrimental zone, mortar bars with optimized PSD stayed in the non-detrimental zone. While 15% FA with non-optimized PSD substituted mortar bars came out to be non-detrimental in terms of ASR, 10% FA addition with optimized PSD was sufficient to make the ASR effect non-detrimental.

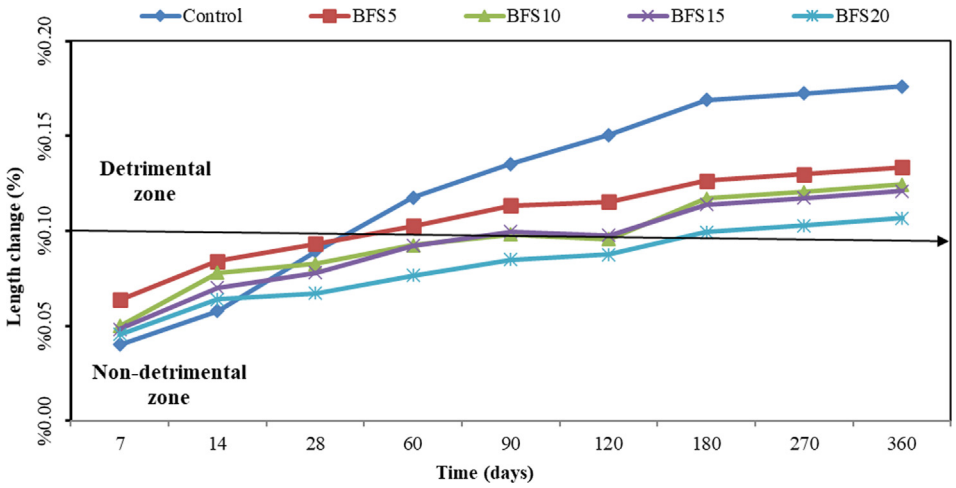

Fig. 3. The length changes of the mortar bar having BFS.

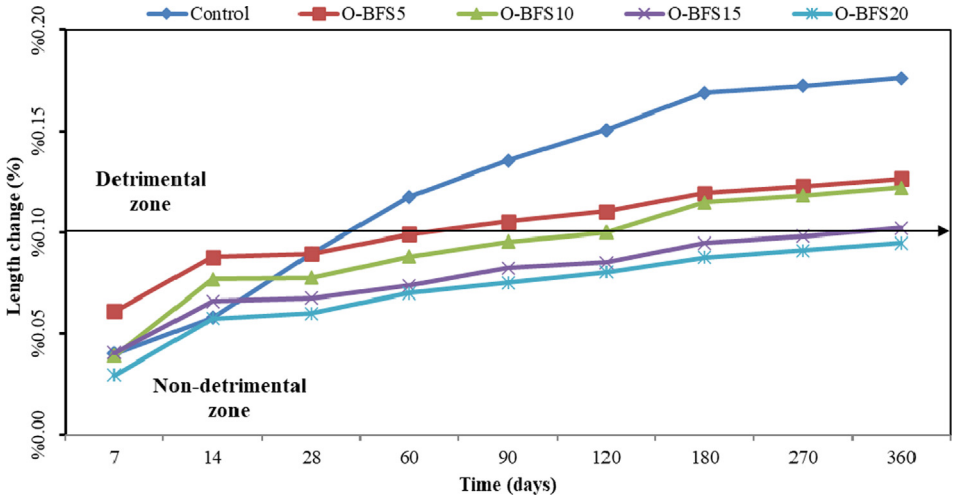

Fig. 4. The length changes of the mortar bar having O-BFS.

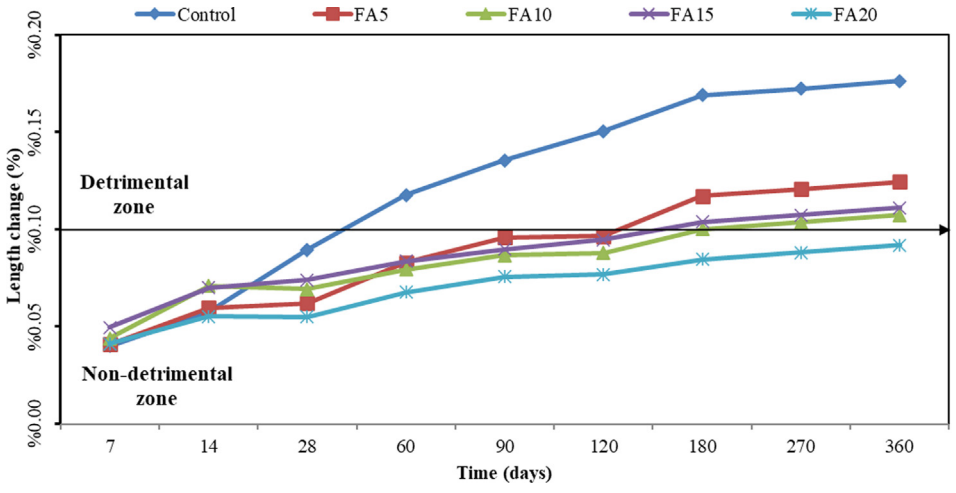

Fig. 5. The length changes of the mortar bar having FA.

According to the experimental results, it was deduced that the optimized PSD of powder materials (FA and BFS) gave the lowest expansion in terms of composites resulting in decreases in length change values for all curing ages, regardless of the replacement ratio of FA and BFS. Cement-based composites containing PSD-optimized FA and BFS exhibited better performances as compared

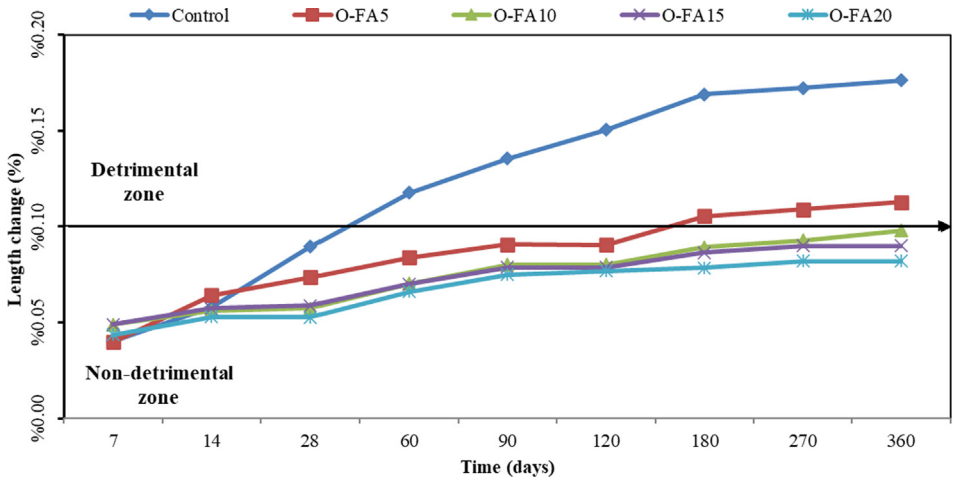

Fig. 6. The length changes of the mortar bar having O-FA.

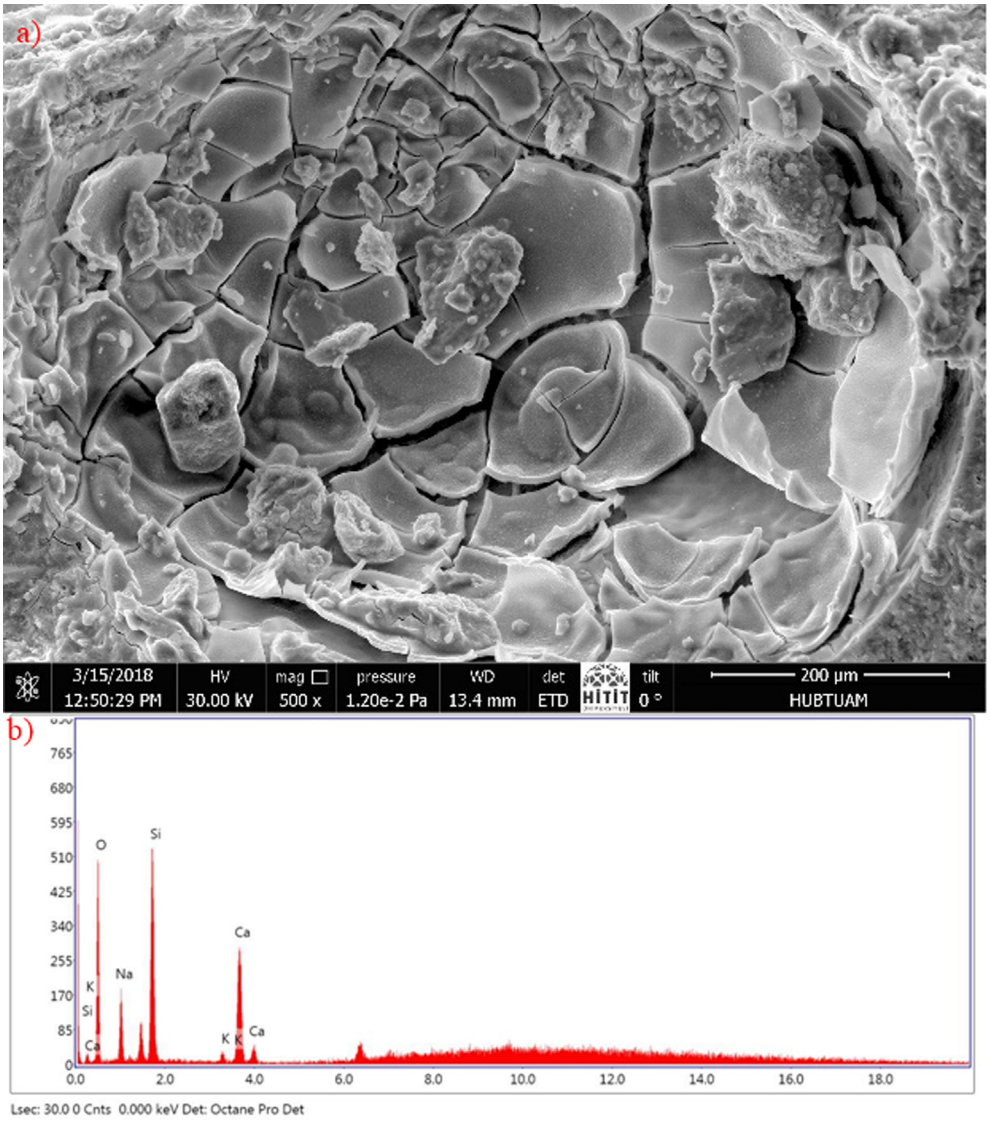

Fig. 7. Control specimen: (a) SEM image of ASR formation (b) EDS spectrum of the mortar.

to cement-based composites containing non-optimized fly ash particles. Thus, it can be revealed that the optimization process for PSD of FA and BFS particles enhanced their filler effect and reduced permeability in cementitious composites, thus mitigate to form ASR.

As a result, the mitigation of ASR on cementitious composites improved by providing optimized PSD of fly ash and blast furnace slag resulting in maximum particle packing. By optimization of PSD of fly ash and blast furnace slag, the amount of cement required for the same target will decrease and utilization of fly ash and blast furnace slag as a waste material will increase.

3.3. Characterization of the test results of specimens

3.3.1. Microstructural properties of specimens having FA and BFS with and without optimization under the ASR effect

In the images obtained from the scanning electron microscope (SEM), it was observed that ASR products were generally situated between aggregate-cement paste in the cavities. ASR products with different morphological structures were clearly visible on images of approximately 100× or higher magnification. As a result of examinations conducted, alkali-silica formations can clearly be seen in Fig. 7 which is given for control specimen. Examinations conducted on the control specimen; ASR findings were found in the form of large cracks in approximately 100 μm dimensions. Cracks generally started in a hollow structure and spread around the cavity. ASR cracks appear in the areas where these cavities occurred, and cracks were concentrated in between 2 and 10 μm. In general, cracks formed in the form of map type cracks and gel formation clearly indicated the presence of ASR observationally. In Fig. 7, it can be seen that massive products with a diameter of 25 to 50 μm are formed as layers.

In the case of mortar bars of 20% BFS addition with non-optimized PSD, ASR findings were in the form of corn flake type and map type cracks. These findings are given in Fig. 8. The existence of ASR was formed in the form of map type cracks for the in cavities larger than 80 μm and in the form of map type and corn flake type in cavities of 300 μm and larger.

When cement mortar bars of 20% BFS with optimized PSD are examined with SEM, the effects of ASR occurred as map type cracks with 1–1.5 μm thicknesses, as can be seen in Fig. 9.

In the examinations, the effects of ASR under 1000× magnification were found in mortar bars of 20% FA (Fig. 10). ASR products were observed in the form of a corn flake type with a distribution

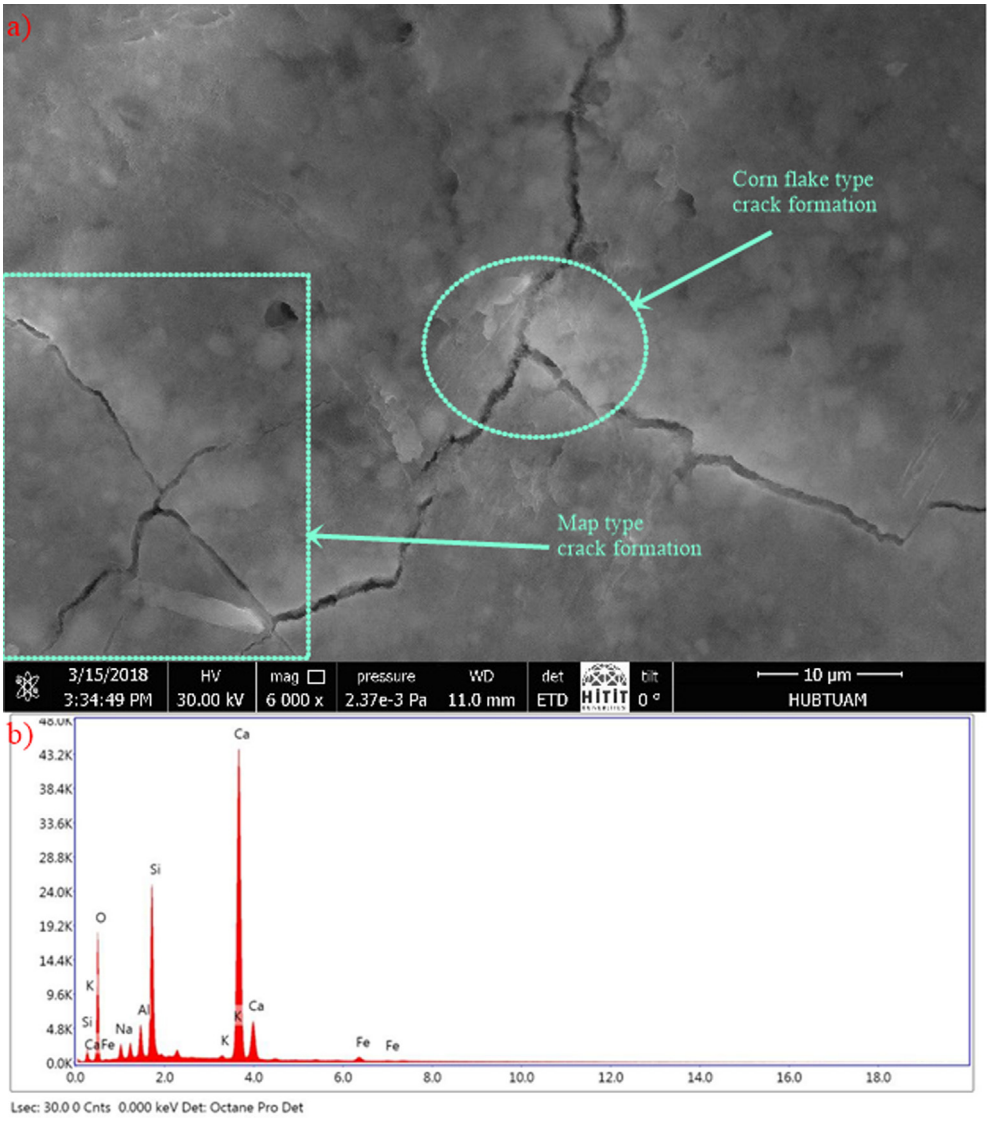

Fig. 8. Specimen having 20% BFS: (a) SEM image of ASR formation (b) EDS spectrum of the mortar.

of approximately 30 μm, and also map type cracks were also found as the effect of ASR. It has been observed that these cracks continued along cavities of 1–3 μm in thickness and 400–600 μm in dimensions.

SEM image obtained for mortar bars of 20% FA with optimized PSD is given in Fig. 11. As a result of observations made, ASR occurrences were encountered under 2000×, while map type cracks showing ASR occurrences were encountered under 8000× magnification. ASR products were observed under 2000× magnification in ASR cavities formed in distribution of approximately 200 μm, but cracks due to these products were able to be seen at 8000× magnification.

As compared to other BFS and FA substituted mortar bars, a less cavity-structure were encountered on the surface of mortar bars of 20% FA addition with optimized PSD. Cracks occurring in cavities with approximately 200 μm in diameter were approximately 0.5–1 μm thick and non-continuous.

SEM image for mortar bar of 20% O-FA is given in Fig. 11. Although ASR effect is considered to be observed in SEM images, it was almost non-existent.

As can be seen from the SEM image given in Fig. 11, the effects of ASR can be observed in images under larger magnification as the FA or BFS addition ratio increase in mortar bars. This phenomenon indicates that the ASR effect increases as the pozzolan addition ratio decreases and the ASR effect decreases as the addition ratio increases. In other words, as FA or BFS addition ratio increases, the effect of ASR decreases. In SEM studies, it was observed that the width of cracks caused by ASR decreased as pozzolan addition ratio increased and as carrying out PSD optimization. This clearly shows that the optimization of PSD of FA and BFS reduces the effect of ASR. ASR formation and its effects were mostly observed in control specimens without puzzolan addition and were at least observed in mortar bars of 20% FA with optimized PSD. From the tests of mortar bars prepared, it was found that 20% FA with optimized PSD was most effective in reducing the effect of ASR.

As can be seen from the EDS analysis given in Table 4, the EDS analysis of control (base) specimen subjected to ASR yielded a high SiO_2 ratio. The SiO_2 ratio was obtained as 50.2%, CaO as 22.2% for the control specimen. The EDS analysis of specimens containing 20% O-BFS yielded a high CaO ratio. The CaO ratio was obtained as 83.9% and SiO_2 as 14.7% for specimen with 20% O-BFS. The EDS analysis of specimens containing 20% BFS yielded high CaO and SiO_2 ratio. The CaO ratio was obtained as 52.2% and SiO_2 as 34.8% for specimen with 20% BFS. The EDS analysis of specimens

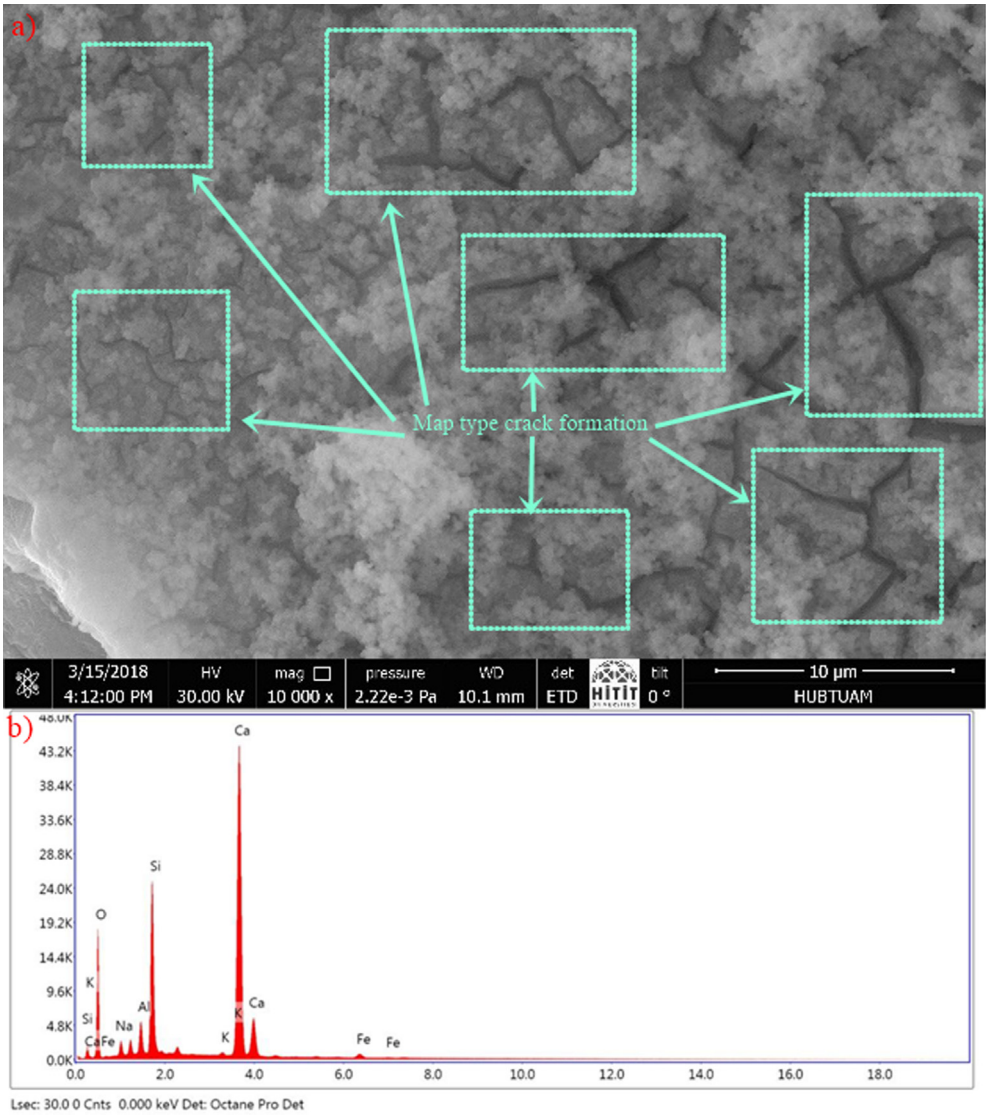

Fig. 9. Specimen having 20% O-BFS: (a) SEM image of ASR formation (b) EDS spectrum of the mortar.

containing 20% O-FA yielded high CaO. The CaO ratio was obtained as 67% and SiO_2 as 22.7% for specimen with 20% O-FA. The EDS analysis of specimens containing 20% FA yielded a high CaO and SiO_2 ratio. The CaO ratio was obtained as 37.9% and SiO_2 as 42.7% for specimen with 20% FA. As a result of EDS analyses, it is proved that the specimens with high SiO_2 ratio have more ASR. As presented above, SiO_2 ratio in ASR gels decreased with an increasing amount of optimized fly ash and blast furnace slag ratio.

3.3.2. Fourier transform infrared spectroscopy (FTIR) of specimens with and without optimized fly ash under the ASR effect

FTIR spectra of specimens with and without optimized fly ash additive (Fig. 12) are shown in Fig. 13 where intense peaks are observed for the wavenumber value ranging in between 400 and 4000 cm^{-1}. Table 5 indicates possible assignments for the bands determined in the Fourier transform infrared spectroscopy spectrum shown in Fig. 13. The specimen with non-optimized FA shows intense SiO_4 and CO_4 bands ranging in between 436 and 889 cm^{-1}. In specimen with non-optimized FA, the structure of the bands are considerably greater than specimen with 20% O-FA addition; which can indicate more alkali solution. The peak of the wide polymerized silica band (786–1017 cm^{-1}) is observed in the specimen with non-optimized FA. The sharper peak within the polymerized silica band has been informed previously in the literature in specimens subjecting accelerated ASR [35,37].

3.3.3. Thermogravimetric analysis (TGA) of specimens having optimized and non-optimized fly ash under the ASR effect

Thermogravimetric analysis (TGA) of specimens with and without optimized fly ash additive is shown in Fig. 14. The weight loss of the specimen with non-optimized FA and specimen with 20% O-FA additive in Thermogravimetric analysis (TGA) is very similar, showing a similar amount of bound water in the hydration gels. TGA curves of the specimen with non-optimized FA and specimen with 20% O-FA additive showed a mass loss of 13.01% and 9.82%, respectively. The mass loss of 8.066% and 5.577% was observed up to 400 °C for the specimen with non-optimized FA and specimen with 20% O-FA additive, respectively. The mass loss of 3.72% and 2.745% was observed between 500 and 1000 °C for the specimen with non-optimized FA and specimen with 20% O-FA additive, respectively. Moropoulou et al. [42] and Abbas et al. [43] observed mass loss due to a decrease in the Calcium hydroxide (CH) content and decarbonation reactions. Various researchers [43–45] also reported a reduction in ASR expansion due to decrease amount

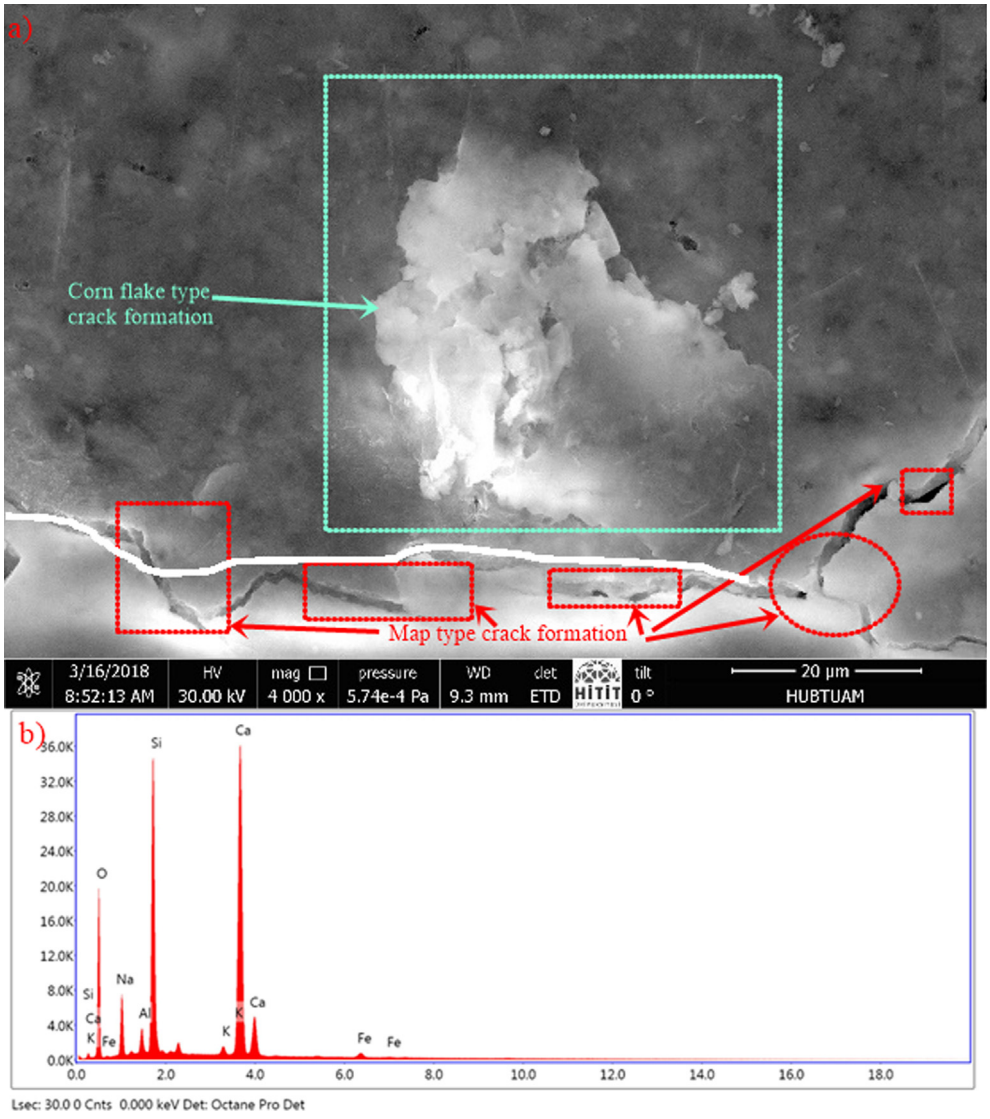

Fig. 10. Specimen having 20% FA: (a) SEM image of ASR formation (b) EDS spectrum of the mortar.

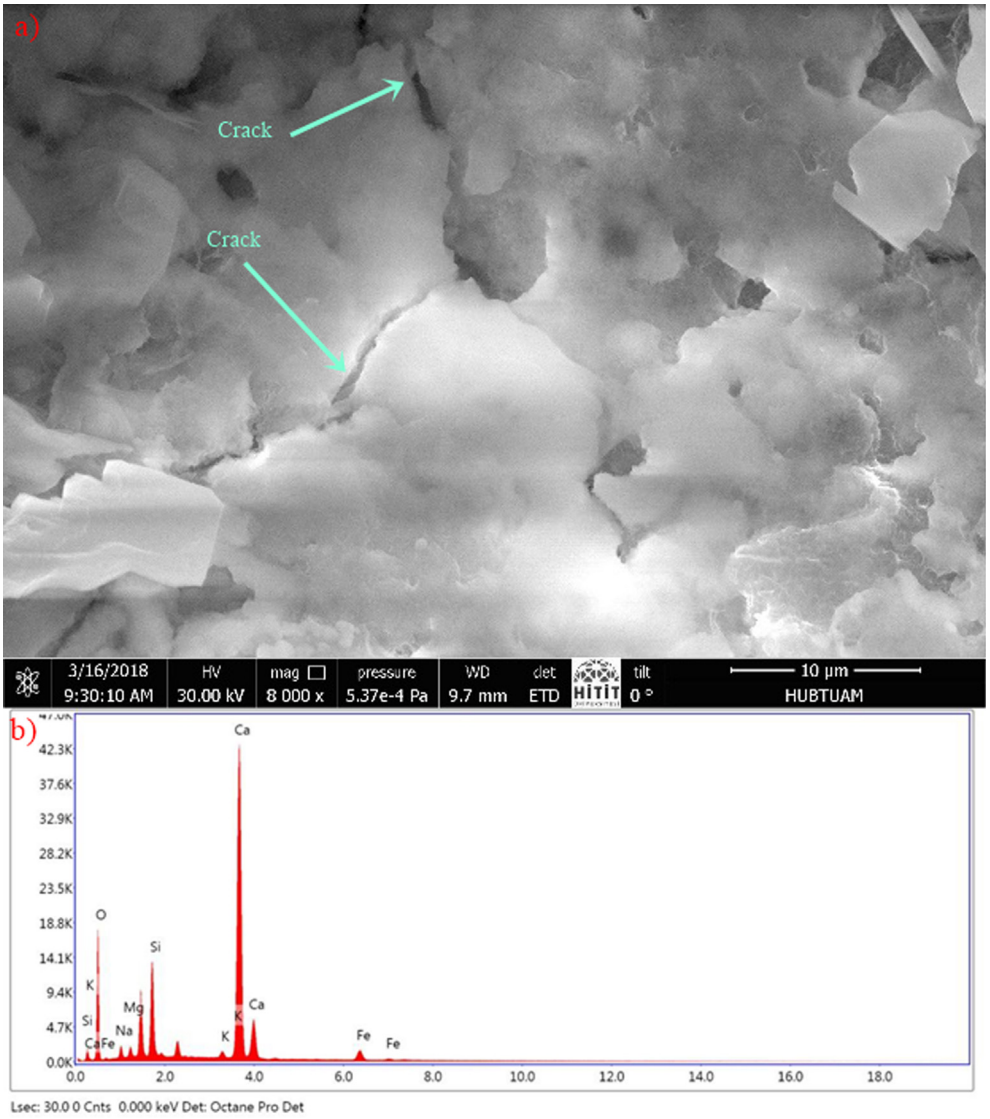

Fig. 11. Specimen having 20% O-FA: (a) SEM image of ASR formation (b) EDS spectrum of the mortar.

Table 4
EDS analysis of control (base), 20% O-BFS, 20% BFS, 20% FA and 20% O-FA added specimens.

Compound (%)	Control	20% O-BFS	20% BFS	20% O-FA	20% FA
CaO	22.2	83.9	52.2	67.0	37.9
SiO_2	50.2	14.7	34.8	22.7	42.7
MgO				2.2	
Na_2O	26.4	1.2	6.4	6.1	15.8
Al_2O_3			6.1		2.9
K_2O	1.2	0.2	0.5	0.3	0.4
Fe_2O_3				1.7	0.4

of CH. Higher CH content can increase the ASR expansion by switching the hydration products' characteristics [46]. Fig. 14 shows that the specimen with non-optimized FA has more ASR expansion due to CH intense. This result is compatible with the EDS analysis, FTIR analysis, and length changes.

4. Conclusion

In this study, tests were conducted for further reduction in the ASR effect, which can be observed in structures, by use of pozzolans with optimized particle size distribution. To this end, cementitious composites was substituted by two different pozzolans, namely FA and BFS, with optimized and non-optimized particle size distribution and the results obtained were discussed comparatively. Following results were reached as a result of this study:

- It has been observed that mortar bar specimens produced with blast furnace slag (BFS) and fly ash (FA) reduces alkali silica reaction (ASR).

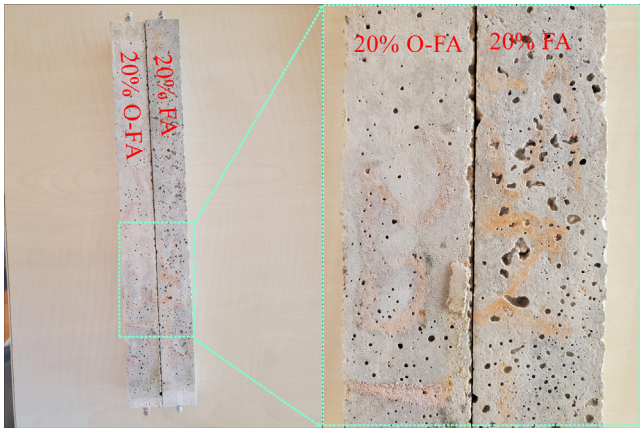

Fig. 12. Specimens (a) having 20% O-FA (b) having 20% FA.

- According to ASTM C1260; in the case of specimens produced with fly ash (FA) with non-optimized particle size distribution was found to be non-detrimental in terms of ASR for 15–20% addition rates. The amount of fly ash (FA) required to make the ASR effect non-detrimental reduced to 10% by addition of fly ash (FA) with optimized particle size distribution (PSD).
- According to ASTM C1260; in the case of specimens produced with blast furnace slag (BFS) with non-optimized particle size distribution were in the detrimental zone in terms of ASR, 5–15% blast furnace slag (BFS) with optimized particle size distribution (PSD) substituted specimens were stayed in the controlled zone and 20% substituted ones remained in the non-detrimental zone in terms of ASR.
- In the experiments performed according to ASTM C227; it has been observed that mortar bars having 20% blast furnace slag (BFS) with optimized particle size distribution (PSD), by 15–20% fly ash (FA) with non-optimized particle size distribution and by 10–20% fly ash (FA) with optimized particle size distribution came out to be in the non-detrimental zone in terms of ASR.

Table 5
Possible assignment of identified FTIR Peak.

Wavenumber (cm^{-1})	Possible Assignment	References
436–588	SiO_4	[34,35]
691	CO_3	[34–36]
786	SiO_4	[34–41]
889	CO_3	[34–36]
1017	SiOH	[40,41]
1055–1300	SO_4	[34–36]
1650	H_2O	[34–36]
3450	H_2O	[34–36]
3500	CH	[34–36]

- As a result of the experimental studies conducted according to ASTM C1260 and ASTM C227, the maximum length change was observed in the control specimens whereas the minimum length change was obtained in mortar bars of 20% fly ash (FA) addition with optimized particle size distribution. As a result, control specimen faced the highest ASR damage whereas specimen with 20% fly ash (FA) addition with optimized particle size distribution faced the lowest damage.
- It has been found out that optimizing the particle size distribution of FA and BFS is more effective in reducing the effects of alkali silica reaction.
- According to microstructural investigations made using scanning electron microscope; map type cracks and corn flake type expansions were encountered in the lower magnification images of mortar bars with high length change due to alkali silica reaction while they were encountered in the higher magnification images of mortar bars with low length change. This shows us that microstructurally larger alkali silica reaction damages occur in mortar bars with higher length change.
- SEM, FTIR and TGA test results showed that more expansion occurred due to ASR in control specimen. EDS analysis of specimens showed that SiO_2 was higher in specimens with non-optimized additives.

As a result, the effect of optimizing the particle size distribution FA and BFS in reducing the formation of ASR is due to the increase in filling effect which reduces the void ratio and permeability in

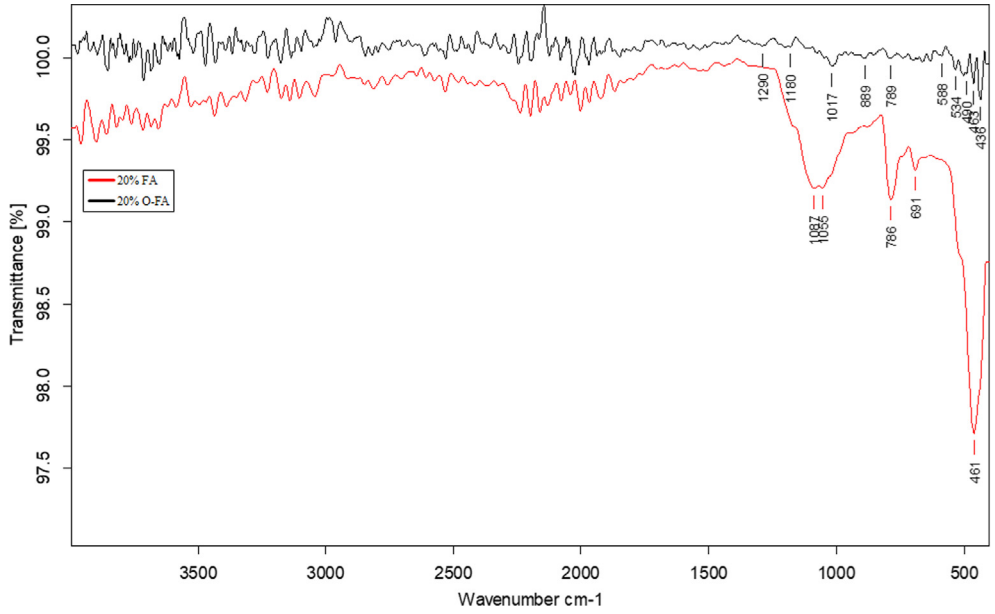

Fig. 13. FTIR spectra of specimens with and without optimized FA.

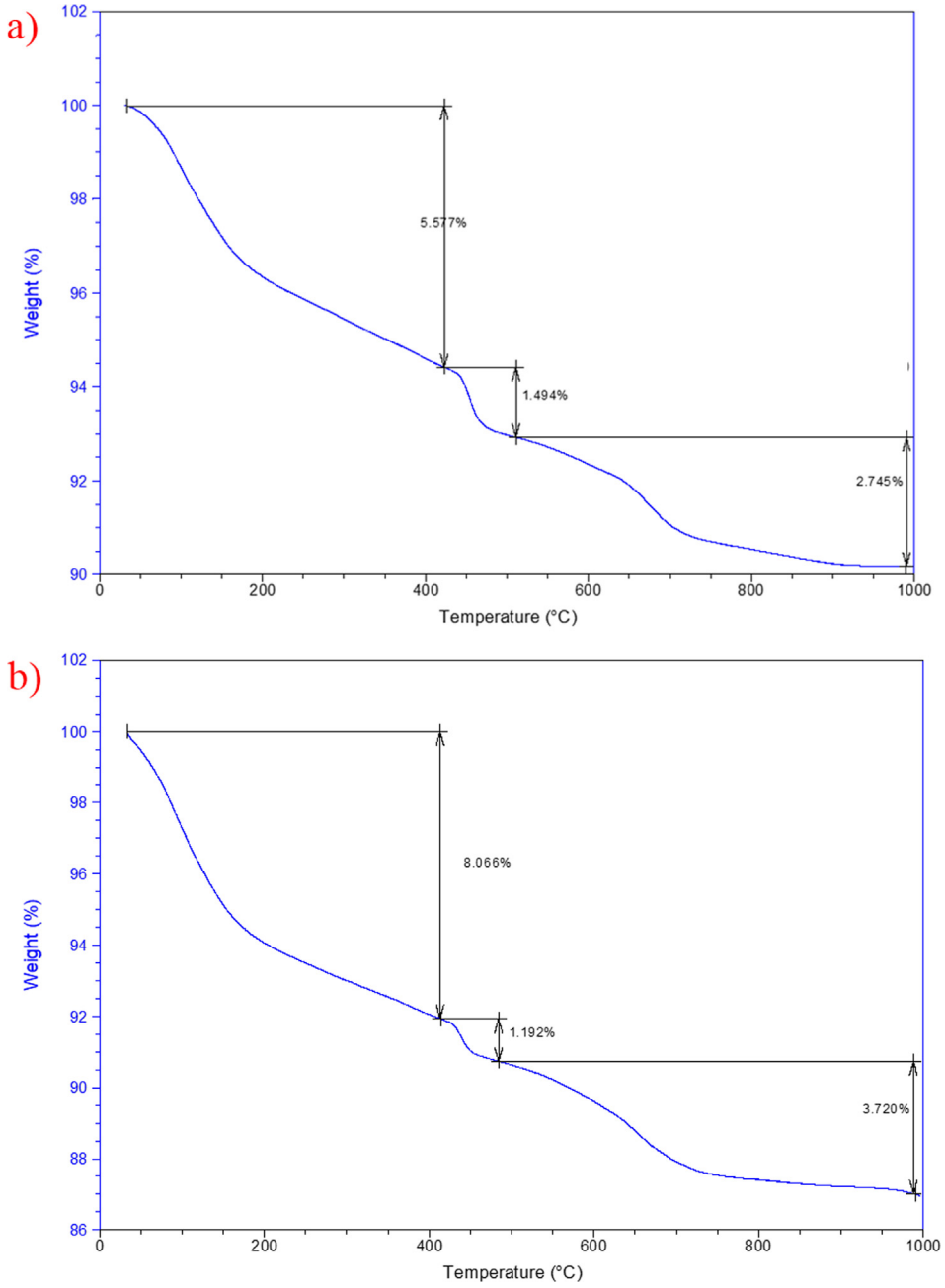

Fig. 14. TGA curves of specimens: (a) having 20% O-FA (b) having 20% FA.

cement mortar bars. Considering the cement mortar bars of 20% FA addition with optimized particle size distribution, it can be concluded that mortar substituted by FA reduces the effects of alkali silica reaction (ASR) almost to zero. By this way, 20% cement can be saved, and the effects of alkali silica reaction can be neutralized.

CRediT authorship contribution statement

İlhami Demir: Investigation, Methodology, Writing - review & editing, Supervision. **Burak Sivrikaya:** Conceptualization, Methodology, Investigation, Visualization, Writing - original draft. **Ozer Sevim:** Conceptualization, Methodology, Investigation, Writing - review & editing, Supervision. **Mehmet Baran:** Writing - review & editing.

Declaration of Competing Interest

The authors declare that they have no known competing financial interests or personal relationships that could have appeared to influence the work reported in this paper.

References

[1] İ. Demir, Ö. Sevim, İ. Kalkan, Microstructural properties of lithium-added cement mortars subjected to alkali–silica reactions, Sādhanā 43 (7) (2018), https://doi.org/10.1007/s12046-018-0901-3.
[2] T.C. Esteves, R. Rajamma, D. Soares, A.S. Silva, V.M. Ferreira, J.A. Labrincha, Use of biomass fly ash for mitigation of alkali-silica reaction of cement mortars, Constr. Build. Mater. 26 (1) (2012) 687–693.
[3] M.H. Shehata, M.D.A. Thomas, Use of ternary blends containing silica fume and fly ash to suppress expansion due to alkali–silica reaction in concrete, Cem. Concr. Res. 32 (3) (2002) 341–349.

[4] ASTM C125, Standard Terminology Relating to Concrete and Concrete Aggregates, ASTM International, New York, 1994.
[5] Franco Massazza, Pozzolanic cements, Cem. Concr. Compos. 15 (4) (1993) 185–214.
[6] R.N. Swamy, Cement Replacement Materials, Surrey University Press, London, 1986.
[7] N Bouzoubaâ, M.H Zhang, V.M Malhotra, Mechanical properties and durability of concrete made with high-volume fly ash blended cements using a coarse fly ash, Cem. Concr. Res. 31 (10) (2001) 1393–1402.
[8] İlhami Demir, Özer Sevim, Effect of sulfate on cement mortars containing Li2SO4, LiNO3, Li2CO3 and LiBr, Constr. Build. Mater. 156 (2017) 46–55.
[9] İlhami Demir, Metin Arslan, The mechanical and microstructural properties of Li2SO4, LiNO3, Li2CO3 and LiBr added mortars exposed to alkali-silica reaction, Constr. Build. Mater. 42 (2013) 64–77.
[10] ASTM C618-19, Standard Specification for Coal Fly Ash and Raw or Calcined Natural Pozzolan for Use as a Mineral Admixture in Concrete.
[11] Michael Thomas, Andrew Dunster, Philip Nixon, Barry Blackwell, Effect of fly ash on the expansion of concrete due to alkali-silica reaction – exposure site studies, Cem. Concr. Compos. 33 (3) (2011) 359–367.
[12] Vanchai Sata, Chai Jaturapitakkul, Kraiwood Kiattikomol, Influence of pozzolan from various by-product materials on mechanical properties of high-strength concrete, Constr. Build. Mater. 21 (7) (2007) 1589–1598.
[13] N.P. Hasparyk, P.J. Monteiro, H. Carasek, Effect of silica fume and rice husk ash on alkali-silica reaction, ACI Mater. J. 97 (4) (2000) 486–492.
[14] D. Ravina, P.K. Mehta, Compressive strength of flow cement/high fly ash concrete, Cem. Concr. Res. 18 (1986) 571–583.
[15] A.K. Saha, M.N.N. Khan, P.K. Sarker, F.A. Shaikh, A. Pramanik, A. The ASR mechanism of reactive aggregates in concrete and its mitigation by fly ash: A critical review, Constr. Build. Mater. 171 (2018) 743–758.
[16] L.J. Malvar, L.R. Lenke, Efficiency of fly ash in mitigating alkali-silica reaction based on chemical composition, ACI Mater. J. 103 (5) (2006) 319.
[17] Medhat H. Shehata, Michael D.A. Thomas, Roland F. Bleszynski, The effects of fly ash composition on the chemistry of pore solution in hydrated cement pastes, Cem. Concr. Res. 29 (12) (1999) 1915–1920.
[18] E. Schäfer, Einfluss der Reaktionen verschiedener Zementhauptbestandteile auf den Alkalihaushalt der Porenlösung des Zementsteins (Doctoral dissertation, Verlag nicht ermittelbar), Technischen Universität Clausthal, Düsseldorf, 2004.
[19] L Lam, Y.L Wong, C.S Poon, Effect of fly ash and silica fume on compressive and fracture behaviors of concrete, Cem. Concr. Res. 28 (2) (1998) 271–283.
[20] O.E. Manz, Coal fly ash: a retrospective and future look, Fuel 78 (2) (1999) 133–136.
[21] İlhami Demir, Selahattin Güzelkücük, Özer Sevim, Effects of sulfate on cement mortar with hybrid pozzolan substitution, Eng. Sci. Tech. Int. J. 21 (3) (2018) 275–283.
[22] Prinya Chindaprasirt, Chai Jaturapitakkul, Theerawat Sinsiri, Effect of fly ash fineness on compressive strength and pore size of blended cement paste, Cem. Concr. Compos. 27 (4) (2005) 425–428.
[23] S.J. Barnett, M.N. Soutsos, S.G. Millard, J.H. Bungey, Strength development of mortars containing ground granulated blast-furnace slag: Effect of curing temperature and determination of apparent activation energies, Cem. Concr. Res. 36 (3) (2006) 434–440.
[24] Ge Zhang, Guoxin Li, Effects of mineral admixtures and additional gypsum on the expansion performance of sulphoaluminate expansive agent at simulation of mass concrete environment, Constr. Build. Mater. 113 (2016) 970–978.
[25] S.J. Kim, K.H. Yang, G.D. Moon, Hydration characteristics of low-heat cement substituted by fly ash and limestone powder, Materials 8 (9) (2015) 5847–5861.
[26] S.J. Choi, S.S. Lee, P.J. Monteiro, Effect of fly ash fineness on temperature rise, setting, and strength development of mortar, J. Mater. Civ. Eng. 24 (5) (2012) 499–505.
[27] T.R. Naik, S.S. Singh, Influence of fly ash on setting and hardening characteristics of concrete systems, ACI Mater. J. 94 (1997) 355–360.
[28] Özer Sevim, İlhami Demir, Physical and permeability properties of cementitious mortars having fly ash with optimized particle size distribution, Cem. Concr. Compos. 96 (2019) 266–273.
[29] Özer Sevim, İlhami Demir, Optimization of fly ash particle size distribution for cementitious systems with high compactness, Constr. Build. Mater. 195 (2019) 104–114.
[30] Ahmet Filazi, İlhami Demir, Ozer Sevim, Enhancement on mechanical and durability performances of binary cementitious systems by optimizing particle size distribution of fly ash, Archiv.Civ.Mech.Eng 20 (2) (2020), https://doi.org/10.1007/s43452-020-00061-x.
[31] ASTM C227-10, Standard Test Method for Potential Alkali Reactivity of Cement-Aggregate Combinations (Mortar-Bar Method). ASTM International, West Conshohocken, PA, 2010.
[32] ASTM C1260-14, Standard Test Method for Potential Alkali Reactivity of Aggregates (Mortar-Bar Method), ASTM International, West Conshohocken, PA, 2014.
[33] J.E. Funk, D.R. Dinger, J.E.J. Funk, Caol Grinding and Particle Size Distribution Studies for Coal Water Slurries at High Solids Content, Final Report, Empire State Electric Energy Research Corporation (ESEERCO), New York, 1980.
[34] M.Y.A. Mollah, W. Yu, R. Schennach, D.L. Cocke, A Fourier transform infrared spectroscopic investigation of the early hydration of Portland cement and the influence of sodium lignosulfonate, Cem. Concr. Res. 30 (2) (2000) 267–273.
[35] S. Oruji, N.A. Brake, R.K. Guduru, L. Nalluri, Ö. Günaydın-Şen, K. Kharel, E. Ingram, Mitigation of ASR expansion in concrete using ultra-fine coal bottom ash, Constr. Build. Mater. 202 (2019) 814–824.
[36] Rikard Ylmén, Ulf Jäglid, Britt-Marie Steenari, Itai Panas, Early hydration and setting of Portland cement monitored by IR, SEM and Vicat techniques, Cem. Concr. Res. 39 (5) (2009) 433–439.
[37] Amirpasha Peyvandi, Iman Harsini, Daniel Holmes, Anagi M. Balachandra, Parviz Soroushian, Characterization of ASR in concrete by Si29 MAS NMR spectroscopy, J. Mater. Civ. Eng. 28 (2) (2016) 04015096, https://doi.org/10.1061/(ASCE)MT.1943-5533.0001354.
[38] Elias Oliveira Serqueira, Rodrigo Ferreira de Morais, Virgílio Anjos, Maria Jose Valenzuela Bell, Noelio Oliveira Dantas, Effect of Na2O concentration on the lifetime of Er3+-doped sodium silicate glass, RSC Adv. 3 (46) (2013) 24298, https://doi.org/10.1039/c3ra40532j.
[39] P. Yu, R.J. Kirkpatrick, B. Poe, P.F. McMillan, X. Cong, Structure of calcium silicate hydrate (C-S-H): Near-, mid-, and far-infrared spectroscopy, J. Am. Ceram. Soc. 82 (3) (1999) 742–748.
[40] M.G. Garnica-Romo, J.M. Yañez-Limón, M. Villicaña, J.F. Pérez-Robles, R. Zamorano-Ulloa, J. González-Hernandez, Structural evolution of sol–gel SiO2 heated glasses containing silver particles, J. Phys. Chem. Solids 65 (6) (2004) 1045–1052.
[41] Angelos G. Kalampounias, IR and Raman spectroscopic studies of sol–gel derived alkaline-earth silicate glasses, Bull. Mater. Sci. 34 (2) (2011) 299–303.
[42] Antonia Moropoulou, Asterios Bakolas, Eleni Aggelakopoulou, Evaluation of pozzolanic activity of natural and artificial pozzolans by thermal analysis, Thermochim. Acta 420 (1-2) (2004) 135–140.
[43] Safeer Abbas, Syed M.S. Kazmi, Muhammad J. Munir, Potential of rice husk ash for mitigating the alkali-silica reaction in mortar bars incorporating reactive aggregates, Constr. Build. Mater. 132 (2017) 61–70.
[44] P.J.M. Monteiro, K. Wang, G. Sposito, M.C.dos Santos, W.P. de Andrade, Influence of mineral admixtures on the alkali-aggregate reaction, Cem. Concr. Res. 27 (12) (1997) 1899–1909.
[45] H. Wang, J.E. Gillott, Mechanism of alkali-silica reaction and the significance of calcium hydroxide, Cem. Concr. Res. 21 (4) (1991) 647–654.
[46] Roland F. Bleszynski, Michael D.A. Thomas, Microstructural studies of alkali-silica reaction in fly ash concrete immersed in alkaline solutions, Adv. Cem. Based Mater. 7 (2) (1998) 66–78.